SCIENTIFIC REPORTS

OPEN

Received: 19 June 2015
Accepted: 22 October 2015
Published: 19 November 2015

Robust Photocatalytic H_2O_2 Production by Octahedral $Cd_3(C_3N_3S_3)_2$ Coordination Polymer under Visible Light

Huaqiang Zhuang, Lifang Yang, Jie Xu, Fuying Li, Zizhong Zhang, Huaxiang Lin, Jinlin Long & Xuxu Wang

Herein, we reported a octahedral $Cd_3(C_3N_3S_3)_2$ coordination polymer as a new noble metal-free photocatalyst for robust photocatalytic H_2O_2 production from methanol/water solution. The coordination polymer can give an unprecedented H_2O_2 yield of ca. 110.0 mmol•L^{-1}•g^{-1} at pH = 2.8 under visible light illumination. The characterization results clearly revealed that the photocatalytic H_2O_2 production proceeds by a pathway of two-electron reduction of O_2 on the catalyst surface. This work showed the potential perspective of $M_x(C_3N_3S_3)_y$ (M = transitional metals) coordination polymers as a series of new materials for solar energy storage and conversion.

Hydrogen peroxide (H_2O_2) is an environmentally benign oxidant widely applied in the areas of organic synthesis, the pulp and paper industry, and disinfection[1]. It is also a block building of post-fossil energy framework as a new solar fuel[2–5]. However, the traditional anthraquinone method[6], also referred as the indirect process, for H_2O_2 production is contrary to the concept of the modern green chemistry, because it not only involves the multistep reactions of high energy-consuming hydrogenation and oxidation, but also requires large production plants to minimize capital investment and to obtain highly concentrated H_2O_2 to reduce transportation costs. The direct synthesis of H_2O_2 by the noble metal-catalyzed reaction of molecular oxygen with hydrogen has proven to be feasible[7–12], but the high production cost and the unsatisfactory efficiency limited its practical application on-large scale. Moreover, some cares have to be required for safe operation because of the potentially explosive danger of H_2/O_2 mixture. Recently, the photocatalyzed H_2O_2 synthesis has attracted more attention as an "ideal green" technique[13–16]. Without the presence of external H_2, H_2O_2 can be produced on a micromolar order in O_2-saturated water by ultraviolet irradiation of TiO_2[17]. By suppressing the back reaction, the photocatalytic H_2O_2 yield can be upgraded to a millimolar level over a surface-fluorinated TiO_2, but along with a large amount of fluorine contaminant emitted into the aqueous solution[18]. Up to date, much work has devoted to chemically modifying TiO_2 by noble metal loading or nonmetallic doping for H_2O_2 synthesis[19–21]. Carbon nitride (g-C_3N_4) and its related composites modified by the electron-deficient aromatic diimide units were recently shown to be also photocatalytically active for H_2O_2 synthesis under visible light illumination[22–24], but it yielded H_2O_2 only on no more than a micromolar level. Thus, the development of visible-light-driven photocatalysts effective for safe H_2O_2 production on a millimolar and even molar scale remains a formidable challenge.

In natural systems, superoxide dismutases (SODs) are metalloprotein enzymes mildly catalyzed H_2O_2 production by the dismutation of superoxide into oxygen and hydrogen peroxide[25]. SODs including three major families of CuZn-SOD, Fe/Mn-SOD and Ni-SOD are essentially coordination compounds with late transition metal ions as central atoms and proteins as ligand. Inspired by these macromolecular

State Key Laboratory of Photocatalysis on Energy and Environment, College of Chemistry, Fuzhou University, Fuzhou, 350116, P. R. China. Correspondence and requests for materials should be addressed to J.L. (email: jllong@fzu.edu.cn)

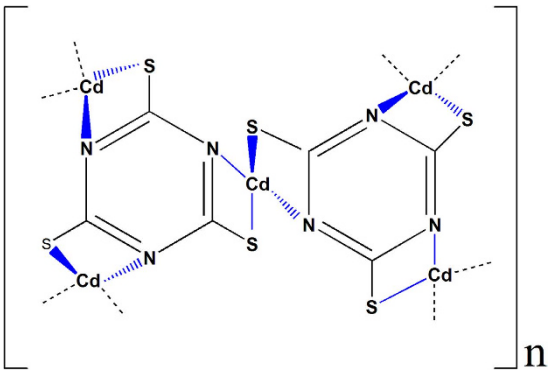

Figure 1. Structure of the $Cd_3(TMT)_2$ coordination polymer.

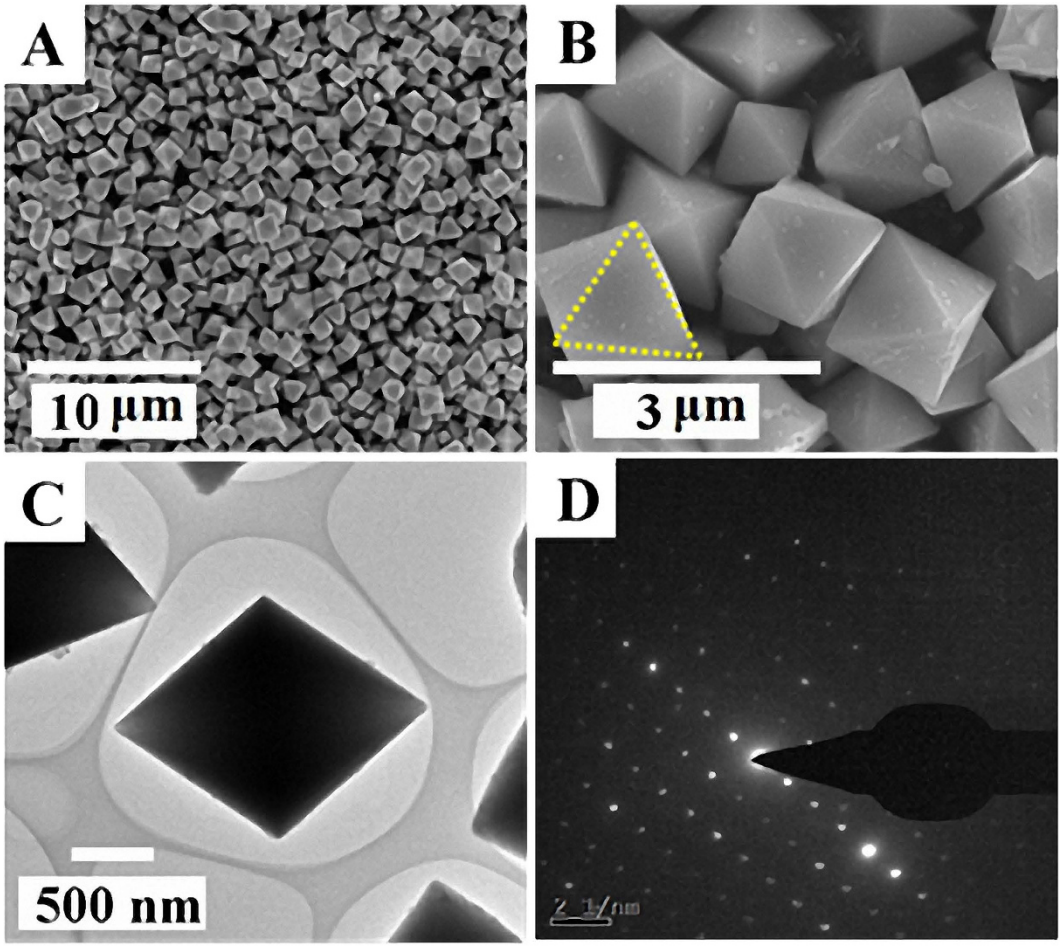

Figure 2. Typical (**A, B**) SEM, (**C**) TEM image and (**D**) the SAED pattern of the $Cd_3(TMT)_2$ coordination polymer.

metalloproteins, we have long looked for metal coordination polymers as robust photocatalysts to mimic the biocatalytic H_2O_2 production. Herein, a $C_3N_3S_3$-based coordination polymer photocatalyst, $Cd_3(C_3N_3S_3)_2$, was successfully developed to produce H_2O_2 on a millimolar level under visible-light irradiation. The yellowish coordination polymer was synthesized by a facile wet-chemical route under the ambient conditions according to the previous work reported by Chudy, J. C. *et al.* who carefully controlled the reaction condition to synthesize the coordination polymer with different stoichiometries[26]. The high stability and low solubility in aqueous solution provided an indicative of the coordination polymer as a catalyst or catalyst support[27]. The elemental analysis of as-synthesed $Cd_3(C_3N_3S_3)_2$ was listed

Entry	pH	hν	Atmosphere	$C(H_2O_2)$ [mmol • L^{-1}]
1[a]	6.7	+	air	negligible
2[b]	6.7	+	air	1.5
3[b]	6.7	−	air	negligible
4[b]	6.7	+	N_2	negligible
5[c]	5.8	+	air	1.75
6[c]	4.1	+	air	2.0
7[c]	2.8	+	air	8.75
8[d]	6.7	+	air	negligible

Table 1. Photocatalytic H_2O_2 evolution over $Cd_3(TMT)_2$ under different conditions. [a] Reaction conditions: 80 mg catalyst dispersed in 20 ml distilled water, visible light ($\lambda \geq 420$ nm), room temperature, the reaction time is 4 hours; [b] Reaction conditions: 80 mg catalyst dispersed in 19 ml distilled water mixed with 1 ml methanol, other conditions as [a]; [c] pH of the solution was adjusted by *con*. HNO_3, other conditions as [b]. [d] With the addition of $AgNO_3$ as electron trapper, other conditions as [b]. The concentration of produced H_2O_2 was determined by $KMnO_4$ titration[20].

in Table S1, which clearly demonstrates that the molar ratio of C, N, S and Cd elements is 1: 0.98: 0.91: 0.55. The result confirms that the general molecular formula of the resultant product is $Cd_3(C_3N_3S_3)_2$, also denoted as $Cd_3(TMT)_2$ where TMT is 2,4,6-trimercaptotriazine anion. The combination of XRD and FTIR characterizations (Fig. S2,S3, Supporting Information) proves the Cd^{2+}-bridged structure of the as-synthesized coordination polymer as depicted in Fig. 1[26–28].

Results and Discussion

Figure 2 shows the low-magnification scanning electron microscopy (SEM) (Fig. 2A,B) and transmission electron microscopy (TEM) images (Fig. 2C) of the as-synthesized $Cd_3(TMT)_2$ coordination polymer. It well crystallizes as homogeneously dispersed nanocrystals with the perfect octahedron morphology characteristics. Additionally, it appears that the triangular surface of these octahedrons is sporadically covered by some irregular-shaped nanoparticles, which suggests that the formation of the octahedral nanocrystals maybe follow the "Oriented attachment" mechanism, just similar to the case of a previous work by Zeng and coworkers[29]. Namely, owing to the strong coordination capability of TMT with transition metal ions as well as the low K_{sp} value of $Cd_3(TMT)_2$ in water[27], the addition of TMT ligand into the Cd^{2+}aqueous solution leads first to the formation of $Cd_3(TMT)_2$ nanoparticular precipitate, and long reaction time endows the self-aggregation of these nanoparticles to construct the final 3D architectures. This hypothesis is confirmed by the SEM images of products at different reaction time as shown in Fig. S4 (Supporting Information). The TEM image in Fig. 2C further evidences that the product are structurally well-defined octahedrons with solid inner space. The selected area electron diffraction pattern (SAED) shown in Fig. 2D indicates the single crystal feature of the coordination polymer.

The ultraviolet-visible diffuse reflectance spectrum of the $Cd_3(TMT)_2$ coordination polymer (Fig. S5, Supporting Information) displays a typical optical absorption of semiconductor. The corresponding to the optical band-gap energy of *ca.* 2.76 eV. To further investigate the band structure of the $Cd_3(TMT)_2$ coordination polymer, we also carried out electrochemical analysis. The typical Mott-Schottky plot of $Cd_3(TMT)_2$ in the dark (Fig. S6, Supporting Information) shows a positive slope of C^{-2}-E plot, an indicative of n-type semiconductor[30]. The flat-band potential (V_{fb}) of about −0.78 V *vs.* NHE at pH 7.0 is determined from extrapolation to the *X* intercept in the Mott-Schottky plot. And by combining with the band-gap energy of ca. 2.76 eV estimated from the optical absorption, the valence band position of the $Cd_3(TMT)_2$ coordination polymer is calculated to be 1.98 V *vs.* NHE at pH 7.0. Thus, it is revealed from the band characteristics as illustrated by the insertion in Fig. S6 that, light-excited electrons in the conduction band of the coordination polymer possess a large thermodynamic driving force to reduce O_2 ($E°(O_2/•O_2^-) = -0.16$ V), and yet the potential of the photogenerated hole in the valence band is inadequate to oxidize OH^- to hydroxyl radicals ($E°(OH^-/•OH) = 2.4$ V). This result clearly indicates that the oxygen reduction reaction over the coordination polymer is feasible.

The activity results of photocatalytic H_2O_2 production from methanol aqueous solution confirm the conclusion above. As listed in Table 1, in pure water (Entry 1), the $Cd_3(TMT)_2$ semiconductor is reluctant to produce H_2O_2 under the indicated conditions. On the contrary, with the addition of methanol as hole scavenger and proton donor, which is beneficial for the separation of electron-hole pairs, 1.5 mmol•L^{-1} H_2O_2 is produced under visible-light irradiation (Entry 2). Notably, this yield is highly comparable to the system using Au-Ag/TiO_2 under ultraviolet light irradiation as previously reported[20]. But in dark (Entry 3), no H_2O_2 is produced, confirming that the H_2O_2 production is driven by light absorption. According to the redox potentials of the electron/hole pairs of the coordination polymer, H_2O_2 can be stoichiometrically formed in an aerated aqueous solution via two different pathways as follows:

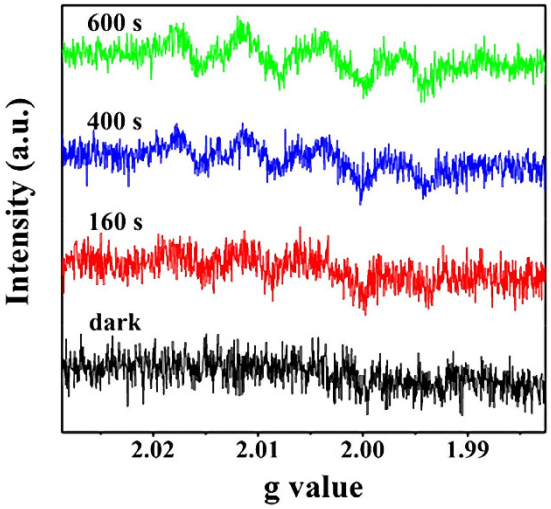

Figure 3. ESR spectra of DMPO–$\bullet O_2^-$/•OOH adduct in the $Cd_3(TMT)_2$/DMPO system before and after visible light irradiation.

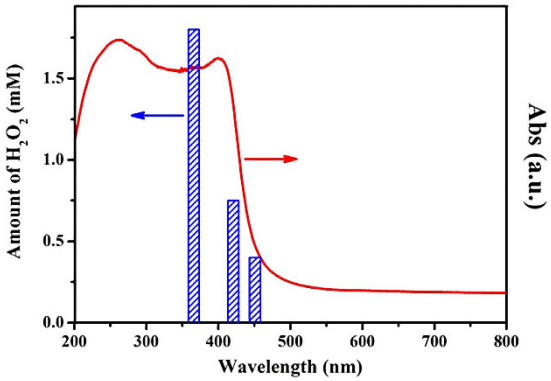

Figure 4. Wavelength-dependent hydrogen peroxide evolution by $Cd_3(TMT)_2$ coordination polymer. Reaction conditions: 80 mg catalyst dispersed in 19 ml distilled water mixed with 1 ml methanol, room temperature. The reaction time is 4 hours.

$$2H^+ + O_2 + 2e^- = H_2O_2 \quad (1)$$

$$2H_2O + 2h^+ = H_2O_2 + 2H^+ \quad (2)$$

Our control experiments uncover some basic mechanism of the $Cd_3(TMT)_2$-catalyzed H_2O_2 evolution. When the system is bubbled with N_2 to eliminate O_2, no H_2O_2 is detected with $KMnO_4$ titration method, indicating the participation of O_2 in the photocatalytic H_2O_2 production. Thus, it can be concluded that the second potential pathway does not contribute to the H_2O_2 production in our system. This conclusion is also confirmed by our further control experiments (Entries 5–7). If water oxidation, as described by equation (2), is primarily responsible for the photocatalytic H_2O_2 production, and then increasing the concentration of H^+will deteriorate the photocatalytic H_2O_2 production of the $Cd_3(TMT)_2$ semiconductor. However, it is shown that, the H_2O_2 concentration increases with the H^+concentration in the solution, and the concentration of H_2O_2 reaches to about 8.75 mmol•L^{-1} at pH = 2.8. In addition, when $AgNO_3$, which is an often-used electron trapper[31], was added in the system (Entry 8), no detectable H_2O_2 is produced in the solution after 4 h of visible-light irradiation. It indicates the pivotal role of photo-electrons for H_2O_2 generation. Based on the activity results of the control experiments we can confirm that, in the case of $Cd_3(TMT)_2$-photocatalyzed H_2O_2 production, the overall reaction would be described by the equation (1), which features two-electron reduction of O_2. It is also noteworthy that, in most cases as previously reported, the produced H_2O_2, a more reactive oxidation agent than O_2, is presumably quick rebound and readily suffers from the reduction reaction by photo-generated electrons

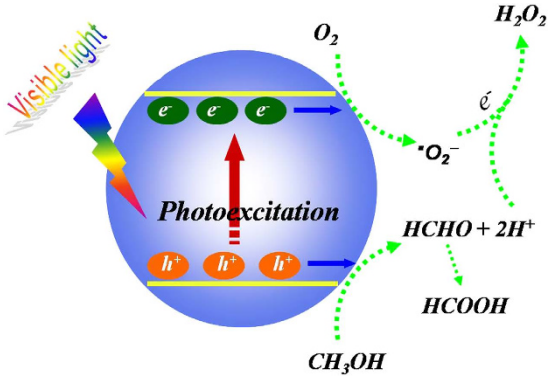

Figure 5. Proposed mechanism of the H_2O_2 production on the visible-light-activated $Cd_3(TMT)_2$ under the ambient condition.

on the catalyst, which results in a very low efficiency of H_2O_2 evolution[21]. Interestingly, in the present study, the accumulation of H_2O_2 with concentration up to several millimoles per liter is achieved. It should be ascribed to the rapid desorption of H_2O_2 from the surface of the $Cd_3(TMT)_2$ photocatalyst, which suppresses the photocatalytic H_2O_2 decomposition.

5,5-dimethyl-1-pyrroline N-oxide (DMPO) trapping electron paramagnetic resonance (ESR) analysis was used to identify the intermediate oxygen species formed during the H_2O_2 evolution, as shown in Fig. 3. No ESR signal can be observed in dark. On the contrary, upon visible light irradiation ($\lambda \geq 420$ nm), a set of ESR signals of DMPO-$\bullet O_2^-$/•OOH adduct ($\bullet O_2^-$, a product derived from oxygen reduction reaction: $O_2 + e^- = \bullet O_2^-$) is discernable within 160 s, and no ESR signals of DMPO−•OH adduct occurs (Fig. S7, Supporting Information), indicating the absence of H_2O_2 decomposition induced by reduction reaction with electrons (*e.g.* $H_2O_2 + e^- = OH^- + \bullet OH$)[32]. Furthermore, the intensity of the DMPO-$\bullet O_2^-$/•OOH adduct signals increase gradually with irradiation time. All these facts are in good agreement with the activity results, indicating that the H_2O_2 evolution over the $Cd_3(TMT)_2$ coordination polymer proceeds *via* the O_2 reduction process, as illustrated by equation (1).

The spectrum action of H_2O_2 production as shown in Fig. 4 further validates that the photoreaction proceeds through light-excitation of the coordination polymer. It appears that the H_2O_2 amount produced in the system decreases with increasing the incident light wavelength, matching well with the optical spectrum. This result clearly indicates that the H_2O_2 production is intrinsically a photocatalytic process driven by photoexcitation of the coordination polymer semiconductor. Therefore, we can propose a reasonable mechanism of $Cd_3(TMT)_2$-photocatalyzed oxygen activation for H_2O_2 production, as illustrated in Fig. 5. Under visible light irradiation, the electron-hole pairs are produced, and then methanol is oxidized by holes into formaldehyde and proton (eq. 3), which contributes to the separation of charge carriers and H^+[33–35]. The adsorbed oxygen molecules are spontaneously reduced by electrons to form superoxide radicals (eq. 4), which further react with protons to produce $\bullet OH_2$ radicals (eq. 5). The $\bullet OH_2$ radicals can readily undergo further reduction with e^- (eq. 6), producing HO_2^- anions. Finally, just as demonstrated by equation (7), the negatively-charged HO_2^- reacts with H^+, leading to the evolution of the final H_2O_2 product[36].

$$CH_3OH + 2h^+ \rightarrow HCHO + 2H^+ \quad (3)$$

$$O_2 + e^- \rightarrow \bullet O_2^- \quad (4)$$

$$\bullet O_2^- + H^- \rightarrow \bullet HO_2 \quad (5)$$

$$\bullet HO_2 + e^- \rightarrow HO_2^- \quad (6)$$

$$HO_2^- + H^+ \rightarrow H_2O_2 \quad (7)$$

In order to clearly verify the photocatalytic reaction mechanism, the concentration of formic acid and formaldehyde has been further measured by the ion chromatography and acetylacetone spectrophotometry, as shown in Fig. S8. The concentration of HCHO and HCOOH gradually increases with the enhancement of reaction time under 24 h of visible-light irradiation, which is good consistent with the above reaction mechanism. Although the accumulated H_2O_2 can further oxidize HCHO into HCOOH, which will lead to some H_2O_2 loss, a stable H_2O_2 concentration in the aqueous solution can be achieved once

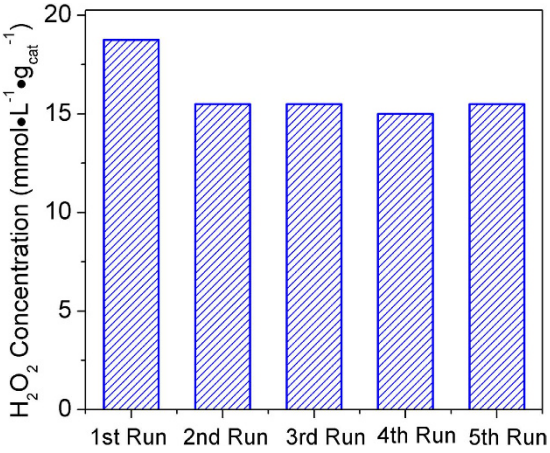

Figure 6. Stability testing of photocatalytic activity of the $Cd_3(TMT)_2$ coordination polymer.

a production-decomposition balance of H_2O_2 is reached, just as demonstrated by Fig. S9 (Supporting Information) representing a time curve of enzyme-biocatalyzed H_2O_2 evolution, over the coordination polymer from methanol aqueous solution. As we all known, the formation and decomposition of H_2O_2 follow zero- and first-kinetics toward H_2O_2 concentration, respectively[14,20]. Therefore, the kinetic data can be modeled and explained by the equation: $[H_2O_2] = (k_f/k_d)\{1\text{-}\exp(1\text{-}k_d t)\}$, where t is time, k_f (mM h^{-1}) and k_d (h^{-1}) are the formation and decomposition rate constants for H_2O_2, respectively. The k_f and k_d values of $Cd_3(TMT)_2$ polymer are 0.39 mM $h^{-1}$and 0.04 h^{-1}, respectively, indicating that the $Cd_3(TMT)_2$ polymer is a robust photocatalyst for H_2O_2 production. To check the photo-stability of the as-prepared photocatalyst, the photocatalytic evolution of H_2O_2 was repeated up to five cycles under the same conditions (Fig. 6). It can be clearly seen that after five successive operations, the coordination polymer still maintains the high photocatalytic activity for H_2O_2 production. In addition, its crystal structure does not change after photocatalytic reaction, as shown in Fig. S10 (Supporting Information). Those results indicate that the $Cd_3(TMT)_2$ polymer is able to serve as a stable, reusable photocatalyst for H_2O_2 generation from methanol/water solution.

According to the characterization results above, we believe that the $Cd_3(TMT)_2$ coordination polymer can fulfill as a versatile visible-light photocatalyst. The activity results of photocatalytic degradation of Rhodamine B over $Cd_3(TMT)_2$ shown in Fig. S11 (Supporting Information) also confirms that it indeed enables the destruction of organic pollutants due to the $\bullet O_2^-$ generation. Importantly, a considerable amount of H_2O_2 is simultaneously produced along with the Rhodamine B photodegradation in the solution[37] (Fig. S12, Supporting Information). This result suggests that the sacrificial agent, methanol, will be hopefully replaced by waste organic dyes for H_2O_2 production in the future, synchronously achievement of environmental remediation.

In summary, a bioinspired metal coordination polymer with a general molecular formula of $Cd_3(TMT)_2$ was reported for the first time to fulfill as a visible light photocatalyst effective for H_2O_2 evolution with the aid of methanol. The coordination polymer features a well-defined octahedral morphology and high crystallinity and shows robust photocatalytic H_2O_2 production on a millimolar level. The electrochemical analysis and ESR characterizations clearly reveal that the photocatalytic H_2O_2 evolution over the coordination polymer follows a mechanism of two-electron reduction of O_2. This work shows the potential promising of the transitional metal coordination polymers in solar energy storage and conversion, especially organic photosynthesis.

Methods

Materials. $Cd(NO_3)_2 \bullet 4H_2O$ and sodium hydroxide (NaOH) were supplied by Sinopharm chemical reagent Co., Ltd (Shanghai, China), trithiocyanuric acid (H_3TMT) was purchased from Tokyo Chemical Industry Co., Ltd (Tokyo, Japan). All materials are analytical grade purity without further purification prior to use. Deionized (DI) water used in the synthesis was obtained from local sources.

Catalyst Preparation. The monodisperse $Cd_3(TMT)_2$ octahedrons are prepared by a facile template-free wet-chemical synthesis at room temperature. Typically, 0.015 mol cadmium nitrate, $Cd(NO_3)_2 \bullet 4H_2O$, was dissolved in 200 mL DI water under mechanically stirring to form a transparent solution (denoted as solution A). Trithiocyanuric acid (0.01 mol) was dissolved in 200 mL 0.15 mol $\bullet L^{-1}$ NaOH aqueous solution to form yellowish homogenous solution, which is denoted as solution B. In order to avoid the formation of cadmium hydroxide precipitation, solution B was slowly added into solution A drop-by-drop under vigorously stirring. Afterwards, the system was aged for 24 h with mildly stirring. The products were then separated by filtration, washed by DI water, and fully dried at 333 K in oven to get the final resultants, namely $Cd_3(TMT)_2$ octahedrons.

Characterizations. The phase composition of the as-prepared samples was determined on a Bruker D8 Advance X-ray diffractometer (XRD) using Ni-filtered Cu Kα radiation at 40 kV and 40 mA in the 2θ ranging from 20° to 80° with a scan rate of 0.02° per second. Field-emission scanning electron microscopy (FE-SEM) was used to characterize the morphology and elemental distribution of the as-prepared samples on a FEI Nova NANOSEM 230 spectrophotometer. Transmission electron microscopy (TEM), high-resolution transmission electron microscopy (HRTEM) images and energy-dispersive X-ray spectroscopy (EDX) were obtained using a JEOL model JEM 2010 EX instrument at an accelerating voltage of 200 kV. The optical properties of the as-prepared samples were analyzed by UV–vis diffuse reflectance spectroscopy (DRS) using a UV–vis spectrophotometer (Cary 500, Varian Co.), in which $BaSO_4$ was employed as the internal reflectance standard. X-ray photoelectron spectroscopy (XPS) measurement was carried out on a Thermo Scientific ESCA Lab 250 spectrometer which consists of a monochromatic Al Kα as the X-ray source, a hemispherical analyzer and sample stage with multi-axial adjustability to obtain the surface composition of the sample. All of the binding energies were calibrated by the C 1 s peak at 284.6 eV. The concentration of formic acid was measured by the ion chromatography (Dionex, ICS-1100). Electron spin resonance (ESR) signal of the radicals spin-trapped by 5,5-dimethyl-l-pyrroline-N-oxide (DMPO) was recorded on a Bruker EPR A300 spectrometer. The irradiation source ($\lambda \geq 420$ nm) was a 300 W Xe arc lamp system and the whole ESR experiment was measured under room temperature. The settings for the ESR spectrometer were as follows: center field = 3507 G, microwave frequency = 9.84 GHz and power = 6.36 mW. The Mott-Schottky experiments were obtained on a Precision PARC workstation. The electrochemical analysis was carried out in a conventional three-electrode cell using a Pt plate and an Ag/AgCl electrode as the counter electrode and reference electrode, respectively. For electrode preparation, indium-tin oxide (ITO) glass was firstly cleaned by sonication in ethanol for 30 min and dried at 353 K. The boundary of ITO glass was protected using scotch tape. 5 mg of sample was dispersed in 0.5 mL ethanol by sonication to get a slurry. The slurry was spread onto the pretreated ITO glass. After air drying, the working electrode was further dried at 393 K for 2 h to improve adhesion. Then the scotch tape was unstuck and the uncoated part of the electrode was isolated with epoxy resin. The exposed area of the working electrode was 0.25 cm^2. Mott-Schottky experiments were measured in a sodium sulfate electrolyte solution (0.2 M) (pH = 6.8), the potential ranged from −0.2 V to 0.8 V, and the perturbation signal were 10 mV with the frequency at 1 K Hz.

Photocatalytic activity test. In a typical photocatalytic reaction, a 300 W Xe arc lamp (PLS-SXE 300, Beijing Perfectlight Co., Ltd.) with a UV−CUT filter to cut off light of wavelength <420 nm was used as the irradiation source. 80 mg of photocatalyst was added into 20 mL of the methanol aqueous solution (19 mL H_2O with 1 mL methanol). Before visible light illumination, the above suspension was stirred in the dark for 1 h to ensure the establishment of adsorption-desorption equilibrium between the sample and reactant. During the process of the reaction, 5 mL of sample solution was collected after 4 hours of visible light irradiation and centrifuged to remove the catalyst completely at 12000 rpm. Afterward, the concentration of H_2O_2 was determined by $KMnO_4$ titration ($c_{KMnO4} = 1\ mmol \bullet L^{-1}$) with the addition of 5 mL 1 M H_2SO_4 solution. When the solution becomes the pink after the addition of $KMnO_4$ solution and keeps the color of solution for 30 s, the concentration of $KMnO_4$ solution is equivalent to the concentration of H_2O_2. All of the experimental processes were conducted under ambient temperature.

References

1. Campos-Martin, J. M., Blanco-Brieva, G. & Fierro, J. L. G. Hydrogen peroxide synthesis: an outlook beyond the anthraquinone process. *Angew. Chem. Int. Ed.* **45,** 6962–6984 (2006).
2. Yamada, Y., Yoneda, M. & Fukuzumi, S. High Power Density of One-Compartment H_2O_2 Fuel Cells Using Pyrazine-Bridged $Fe[MC(CN)_4]$ (MC = $Pt^{2+}$and Pd^{2+}) Complexes as the Cathode. *Inorg. Chem.* **53,** 1272–1274 (2014).
3. Kato, S., Jung, J., Suenobu, T. & Fukuzumi, S. Production of hydrogen peroxide as a sustainable solar fuel from water and dioxygen. *Energy Environ. Sci.* **6,** 3756–3764 (2013).
4. Fukuzumi, S., Yamada, Y. & Karlin, K. D. Hydrogen peroxide as a sustainable energy carrier: Electrocatalytic production of hydrogen peroxide and the fuel cell. *Electrochim. Acta* **82,** 493–511 (2012).
5. Yamada, Y., Yoshida, S., Honda, T. & Fukuzumi, S. Protonated iron–phthalocyanine complex used for cathode material of a hydrogen peroxide fuel cell operated under acidic conditions. *Energy Environ. Sci.* **4,** 2822–2825 (2011).
6. Hess, W. T. In *Kirk-Othemer Encyclopedia of Chemical Engineering*, (Eds. Kroschwitz, I. *et al.*) Ch. 13, 961 (Wiley, New York, 1995).
7. Edwards, J. K. & Hutchings, G. J. Palladium and Gold–Palladium Catalysts for the Direct Synthesis of Hydrogen Peroxide. *Angew. Chem. Int. Ed.* **47,** 9192–9198 (2008).
8. Dissanayake, D. P. & Lunsford, J. H. Evidence for the role of colloidal palladium in the catalytic formation of H_2O_2 from H_2 and O_2. *J. Catal.* **206,** 173–176 (2002).
9. Landon, P., Collier, P. J., Papworth, A. J., Kiely, C. J. & Hutchings, G. J. Direct formation of hydrogen peroxide from H_2/O_2 using a gold catalyst. *Chem. Commun.* 2058–2059 (2002).
10. Edwards, J. K. *et al.* Direct synthesis of H_2O_2 from H_2 and O_2 over gold, palladium, and gold–palladium catalysts supported on acid-pretreated TiO_2. *Angew. Chem. Int. Ed.* **48,** 8512–8515 (2009).
11. Edwards, J. K. *et al.* Switching off hydrogen peroxide hydrogenation in the direct synthesis process. *Science* **323,** 1037–1041 (2009).
12. Lunsford, J. H. The direct formation of H_2O_2 from H_2 and O_2 over palladium catalysts. *J. Catal.* **216,** 455–460 (2003).
13. Zong, X. *et al.* Selective production of hydrogen peroxide and oxidation of hydrogen sulfide in an unbiased solar photoelectrochemical cell. *Energy Environ. Sci.* **7,** 3347–3351 (2014).

14. Kaynan, N., Berke, B. A., Hazut, O. & Yerushalmi, R. Sustainable photocatalytic production of hydrogen peroxide from water and molecular oxygen. *J. Mater. Chem. A* **2,** 13822–13826 (2014).
15. Kormann, C., Bahnemann, D. W. & Hoffmann, M. R. Photocatalytic production of hydrogen peroxides and organic peroxides in aqueous suspensions of titanium dioxide, zinc oxide, and desert sand. *Environ. Sci. Tech*. **22,** 798–806 (1988).
16. Rao, M. V., Rajeshwar, K., Verneker, V. R. P. & DuBow, J. Photosynthetic production of hydrogen and hydrogen peroxide on semiconducting oxide grains in aqueou. *J. Phys. Chem.* **84,** 1987–1991 (1980).
17. Li, X., Chen, C. & Zhao, J. Mechanism of photodecomposition of H_2O_2 on TiO_2 surfaces under visible light Irradiation. *Langmuir* **17,** 4118–4122 (2001).
18. Maurino, V., Minero, C., Mariella, G. & Pelizzetti, E. Sustained production of H_2O_2 on irradiated TiO_2 – fluoride systems. *Chem. Commun.* **0,** 2627–2629 (2005).
19. Teranishi, M., Naya, S.-I. & Tada, H. *In situ* liquid phase synthesis of hydrogen peroxide from molecular oxygen using gold nanoparticle-loaded titanium(IV) dioxide photocatalyst. *J. Am. Chem. Soc.* **132,** 7850–7851 (2010).
20. Tsukamoto, D. *et al.* Photocatalytic H_2O_2 production from ethanol/O_2 system using TiO_2 loaded with Au–Ag bimetallic alloy nanoparticles. *ACS Catal.* **2,** 599–603 (2012).
21. Hirakawa, T. & Nosaka, Y. Selective production of superoxide ions and hydrogen peroxide over nitrogen- and sulfur-doped TiO_2 photocatalysts with visible light in aqueous suspension systems. *J. Phys. Chem. C* **112,** 15818–15823 (2008).
22. Shiraishi, Y., Kanazawa, S., Sugano, Y. & Tsukamoto, D. Highly Selective production of hydrogen peroxide on graphitic carbon nitride (g-C_3N_4) photocatalyst activated by visible light. *ACS. Catal.* **4,** 774–780 (2014).
23. Shiraishi, Y. *et al.* Sunlight-Driven Hydrogen Peroxide Production from Water and Molecular Oxygen by Metal-Free Photocatalysts. *Angew. Chem. Int. Ed.* **53,** 13454–13459 (2014).
24. Shiraishi, Y. *et al.* Effects of Surface Defects on Photocatalytic H_2O_2 Production by Mesoporous Graphitic Carbon Nitride under Visible Light Irradiation. *ACS Catal.* **5,** 3058–3066 (2015).
25. Collén, J., Rio, M., García-Reina, G. & Pedersén, M. Photosynthetic production of hydrogen peroxide by Ulva rigida C. Ag. (Chlorophyta). *Planta* **196,** *2*, 225–230 (1995).
26. Beezer, A. E. & Chudy, J. C. Elucidation of coordination polymer stoichiometry via thermometric titrimetry: metal complexes of trithiocyanuric acid. *Thermochimica Acta* **6,** 231–237 (1973).
27. Matlock, M. M., Henke, K. R., Atwood, D. A. & Robertson, D. Aqueous leaching properties and environmental implications of cadmium, lead and zinc Trimercaptotriazine (TMT) compounds. *Water Res.* **35,** 3649–3655 (2001).
28. Henke, K. R., Bryan, J. C. & Elless, M. P. Structure and powder diffraction pattern of 2,4,6-Trimercapto-s-triazine, trisodium salt ($Na_3S_3C_3N_3{\cdot}9H_2O$). *Powder Diffr.* **12,** 7–12 (1997).
29. Yang, H. G. & Zeng, H. C. Self-construction of hollow SnO_2 octahedra based on two-dimensional aggregation of nanocrystallites. *Angew. Chem.* **116,** 6056–6059 (2004).
30. Kong, D. S. The Influence of fluoride on the physicochemical properties of anodic oxide films formed on titanium surfaces. *Langmuir* **24,** 5324–5331 (2008).
31. Kudo, A., Ueda, K., Kato, H. & Mikami, I. Photocatalytic O_2 evolution under visible light irradiation on $BiVO_4$ in aqueous $AgNO_3$ solution. *Cata. Lett*. **53,** 229–230 (1998).
32. Dou, X. *et al.* Production of superoxide anion radicals as evidence for carbon nanodots acting as electron donors by the chemiluminescence method. *Chem. Commun.* **49,** 5871–5873 (2013).
33. Gu, Q. *et al.* Single-site tin-grafted anatase TiO_2 for photocatalytic hydrogen production: Toward understanding the nature of interfacial molecular junctions formed in semiconducting composite photocatalysts. *J.Catal.* **289,** 88–99 (2012).
34. Gu, Q. *et al.* Ternary Pt/SnO_x/TiO_2 photocatalysts for hydrogen production: consequence of Pt sites for synergy of dual co-catalysts. *Phys. Chem. Chem. Phys.* **16,** 12521–12534 (2014).
35. Gu, Q. *et al.* Single-site Sn-grafted Ru/TiO_2 photocatalysts for biomass reforming: Synergistic effect of dual co-catalysts and molecular mechanism. *J.Catal.* **303,** 141–155 (2013).
36. Carraway, E. R., Hoffman, A. J. & Hoffmann, M. R. Photocatalytic oxidation of organic acids on quantum-sized semiconductor colloids. *Environ. Sci. Tech*. **28,** 786–793 (1994).
37. Bader, H., Sturzenegger, V. & Hoigné, J. Photometric method for the determination of low concentrations of hydrogen peroxide by the peroxidase catalyzed oxidation of N,N-diethyl-p-phenylenediamine (DPD). *Water Res*. **22,** 1109–1115 (1988).

Acknowledgements

We gratefully thank the financial support of the NSFC (Grant Nos 21003021, 21373051, and U1305242), the program for New Century Excellent Talents in Fujian Province University (JA14029), the program for Qishan Scholar of Fuzhou University, and Collaborative Innovation Center of Clean Coal Gasification Technology (XK1401), National Natural Fund of Science Department of Fujian Province (Grant No. 2015J01601).

Author Contributions

H.Q.Z and J.L.L. wrote the manuscript and carried out the most of experiments. L.F.Y., J.X., F.Y.L., Z.Z.Z. and H.X.L. did the ESR and SEM measurements, and obtained the data and figures. J.L.L. and X.X.W. analyzed the data and revised the manuscript. All authors reviewed the manuscript.

Additional Information

Supplementary information accompanies this paper at http://www.nature.com/srep

Competing financial interests: The authors declare no competing financial interests.

How to cite this article: Zhuang, H. *et al.* Robust Photocatalytic H_2O_2 Production by Octahedral $Cd_3(C_3N_3S_3)_2$ Coordination Polymer under Visible Light. *Sci. Rep.* **5**, 16947; doi: 10.1038/srep16947 (2015).